DOI: 10.1002/ejic.201100437

Lanthanide Aminoisophthalate Coordination Polymers: A Promising System for Tunable Luminescent Properties

Yun Luo,[a] Guillaume Calvez,[a] Stéphane Freslon,[a] Kevin Bernot,[a] Carole Daiguebonne,*[a] and Olivier Guillou[a]

Keywords: Coordination polymers / Lanthanides / Polymers / Luminescence

Reactions in water between the disodium salt of 5-amino-1,3-benzenedicarboxylic acid or 5-aminoisophthalate (Na_2aip) and lanthanide chlorides lead to two families of coordination polymers with the respective general chemical formulae $\{[Ln_6(aip)_7(H_2O)_{24}]\cdot 2(aip)\cdot 6H_2O\}_\infty$ in which Ln = Tm or Yb (Family 1) and $\{[Ln_2(aip)_2(H_2O)_{10}]\cdot(aip)\cdot 4H_2O\}_\infty$ in which Ln = La–Er (except Pm) or Y (Family 2). Compounds belonging to Family 1 are isostructural. The crystal structure has been solved for the Er-containing compound. This compound crystallizes in the monoclinic system, space group $P2_1/n$ (n°14) with a = 13.3439(3) Å, b = 27.3332(8) Å, c = 15.7191(4) Å, β = 97.90(1)°, V = 5680.41(82) Å^3 and Z = 4. The crystal structure can be described as the juxtaposition of double helicoidal chains. Additional aminoisophthalate ions insuring the electroneutrality of the network are lying in the interchain space. Compounds belonging to Family 2 are isostructural. The crystal structure has been solved for the Eu-containing compound. This compound crystallizes in the monoclinic system, space group Pn (n°7) with a = 11.3427(2) Å, b = 10.6663(1) Å, c = 15.1639(3) Å, β = 97.8998(9)°, V = 1817.19(5) Å^3 and Z = 2. The crystal structure can be described as the juxtaposition of zigzag double chains. Additional aminoisophthalate ligands are lying in the interchain space insuring the electroneutrality of the network. The luminescent properties under UV irradiation of these compounds have been explored. In particular, quantum yields, lifetimes and colorimetric coordinates of the Tb-, the Sm-, and the Dy-containing coordination polymers have been determined.

Introduction

For almost a decade the number of reported metal organic frameworks (MOF) has rapidly increased.[1–9] This renewal of interest is mainly due to their potential interest for depollution or gas storage purposes. Some of us are currently studying lanthanide-containing coordination polymers, aiming for materials exhibiting porosity[10–13] or interesting luminescent properties[14–16] and are respectful of the environment. Therefore, for more than ten years we have been developing a green synthetic strategy[17] employing water as solvent, non toxic reagents, high-yielding reactions conducted at ambient temperature and pressure, and gel media for crystal growth.[18] We have thus been able to synthesize numerous lanthanide containing coordination polymers involving benzene-polycarboxylate ligands.[19] Actually, benzene-polycarboxylate ligands have drawn much attention[20–22] because they are chemically and thermally stable, present a structuring effect thanks to π-stacking, and the carboxylato functional groups allow one to expect structural diversity due to their numerous possible coordination modes. For example, the V-shaped isophthalic acid ligand is a good spacer and has been widely used in the assembly of coordination polymers.[23–26] The presence of additional groups on the benzene ring can also be used to tailor the properties of the obtained material. For example, the amino group can not only act as a structuring group through strong hydrogen bonds (amino-substituted benzene-polycarboxylate ligands tend to promote 3D molecular structures when associated with lanthanide ions[27–34]) but also, as an electron-donating group, can affect the luminescence properties of the lanthanide containing coordination polymers. We have thus undertaken the study of the aminoisophthalate/Ln^{III} system in water (Scheme 1).

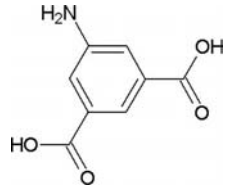

Scheme 1. The aminoisophthalic ligand (5-aminobenzene-1,3-dicarboxylic acid) hereafter referred as H_2aip.

Other families of coordination polymers involving rare earth ions and aminoisophthalate ligands have already been reported. To the best of our knowledge, all have been obtained by hydrothermal methods.[27,35] In this paper, we describe two new families of lanthanide 5-aminoisophthalate coordination polymers with the respective general chemical formulae $\{[Ln_6(aip)_7(H_2O)_{24}]\cdot 2(aip)\cdot 6H_2O\}_\infty$ in which Ln =

[a] INSA, UMR 6226, Sciences Chimiques de Rennes, 35708 Rennes, France
E-mail: carole.daiguebonne@insa-rennes.fr

Tm or Yb (Family 1) and $\{[Ln_2(aip)_2(H_2O)_{10}]\cdot(aip)\cdot 4H_2O\}_\infty$ in which Ln = La–Er (except Pm) or Y (Family 2). All compounds have been obtained in high yield by precipitation in water. The luminescent properties, under UV irradiation, of compounds belonging to Family 2 have been studied.

Results and Discussion

The reactions in water between the disodium salt of 5-amino-1,3-benzene-dicarboxylic acid or 5-aminoisophthalate (Na_2aip) and lanthanide chlorides lead to microcrystalline powders that correspond to two families of coordination polymers depending on the involved lanthanide ion. Their respective general chemical formulae are $\{[Ln_6(aip)_7(H_2O)_{24}]\cdot 2(aip)\cdot 6H_2O\}_\infty$ when Ln = Tm or Yb (Family 1) and $\{[Ln_2(aip)_2(H_2O)_{10}]\cdot(aip)\cdot 4H_2O\}_\infty$ when Ln = La–Er (except Pm) or Y (Family 2). Single crystals of the compounds have been obtained by the slow diffusion through gels in U-shaped tubes or by slow diffusion through water in H-shaped tubes. As often observed, the frontier between Family 1 and Family 2 depends on the synthetic pathway. The obtained phases are summarized in Table 1.

Family 1: $\{[Ln_6(aip)_7(H_2O)_{24}]\cdot 2(aip)\cdot 6H_2O\}_\infty$ in which Ln = Tm or Yb

The crystal structure of the compounds belonging to Family 1 has been solved for the Er-containing single-crystal (Figure 1). The isostructurality of the other compounds of the family has been assumed on the basis of their X-ray diffraction diagrams and single-crystal X-ray diffraction data.

The crystal structure is mono-dimensional and can be described as the juxtaposition of double helicoidal chains (Figure 2) with the chemical formula $[Er_6(aip)_7(H_2O)_{24}]^{4+}$.

These helicoidal chains have the chemical formula $[Er_3(aip)_3(H_2O)_{12}]^{3+}$. They are linked together through a disordered aminoisophthalate ligand that binds Er1 atoms belonging to adjacent chains. The disorder model is illustrated in Figure 3. In this model the bridging aminoisophthalate ligand present two equi-probable orientations. Whatever the orientation, the carboxylate clips O51–C51–O52 remain unchanged and one carbon atom belonging to the phenyl ring (C57) is also present in both orientations of the ligand.

Additional aminoisophthalate ligands insuring the electoneutrality of the network lie in between the double-chain

Table 1. Summary of the syntheses.

	La	Ce	Pr	Nd	Sm	Eu	Gd	Tb	Dy	Ho	Y	Er	Tm	Yb
Powder	Family 2												**Family 1**	
Single Crystals														
gel in U-shaped tube	Family 2													
water in H-shaped tube												**Family 1**		

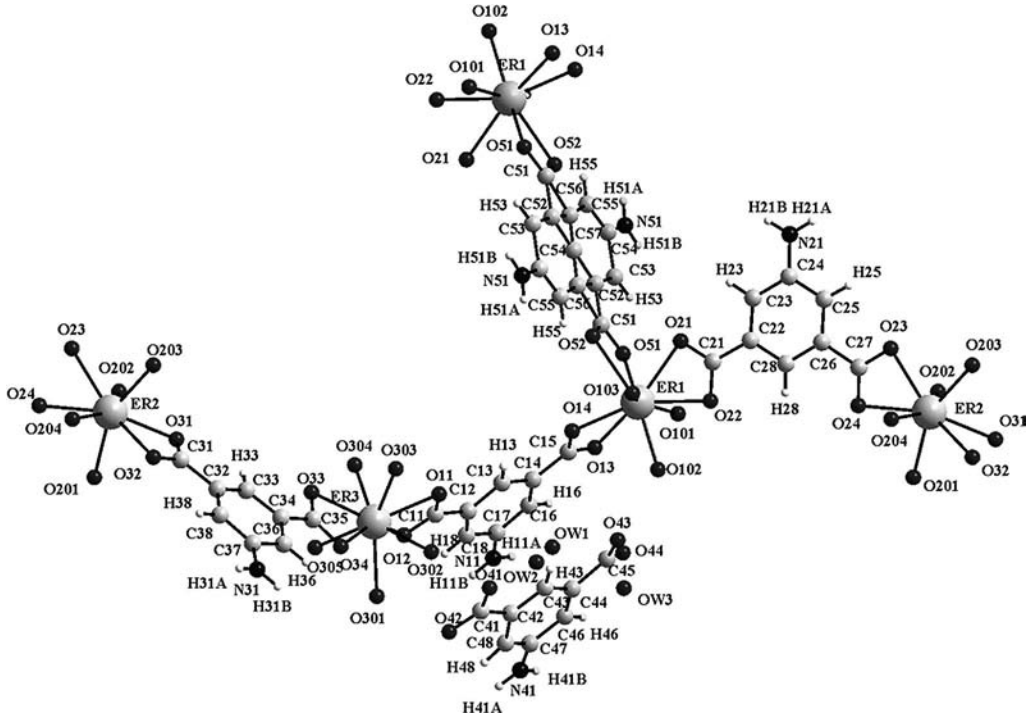

Figure 1. Projection view of an extended asymmetric unit of $\{[Er_6(aip)_7(H_2O)_{24}]\cdot 2(aip)\cdot 6H_2O\}_\infty$.

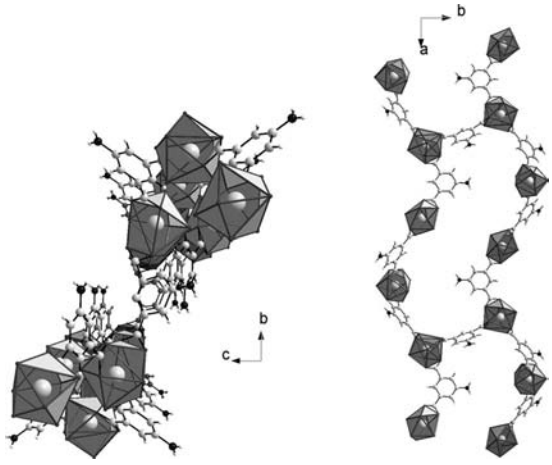

Figure 2. Perspective view along the a axis (left) and projection view along the c axis (right) of the double-helicoidal-chain molecular motif. For clarity, uncoordinated aminoisophthalate ligands and water molecules of crystallization have been omitted.

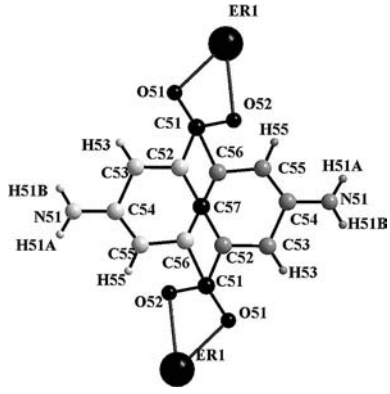

Figure 3. Representation of the disorder model. Atoms in black are present in both orientations of the ligand. Atoms in grey (light or medium) have a half occupancy factor.

molecular motifs. These ligands establish strong intermolecular interactions with the molecular motif through π-stacking[36] with the aminoisophthalate ligand that links the Er1 and Er3 atoms and through hydrogen bonds with water molecules coordinated to Er1 and Er3 (Figure 4). The three water molecules of crystallization are localized in the vicinity of this uncoordinated ligand to which they establish strong hydrogen bonds.

The asymmetric unit contains three crystallographically independent metal ions. The Er1 atom is bound to nine oxygen atoms belonging to three bidentate ligand and three coordinated water molecules, and forms a distorted tricapped trigonal prism. Er3 is bound to nine oxygen atoms from two bidentate ligands and five coordinated water molecules, and forms a distorted tricapped trigonal prism. Lastly, Er2 is bound to only eight oxygen atoms belonging to two bidentate ligands and four coordinated water molecules, and forms a distorted dodecahedron. All the coordinated aminoisophthalate ligands are linked to two Er atoms in a bisbidentate manner. The crystal packing

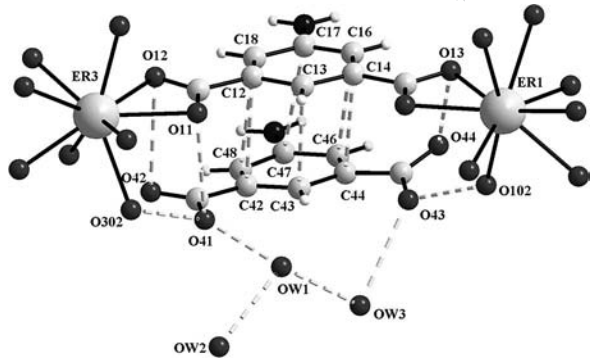

Figure 4. Projection view of the uncoordinated aminoisophthalate ligand, the water molecules of crystallization and a part of the molecular motif. Dotted lines represent intermolecular interactions (π-stacking or H-bond). Selected inter-atomic distances (Å): C17–C47 3.760(6), C18–C48 3.747(7), C12–C42 3.615(7), C13–C43 3.663(7), C14–C44 3.745(6), C16–C46 3.769(6), O44–O13 3.533(5), O43–O102 2.624(6), O41–O302 2.781(7), O41–O11 3.467(8), O42–O12 3.531(8), OW1–O41 2.659(8), OW3–O43 2.822(7), OW1–OW3 2.884(7), OW1–OW2 2.760(3).

is rather compact and presents no significant potential porosity.

The thermal properties of these compounds have been studied both by coupled thermo-gravimetric and thermo-differential analyses (TG/TD) (the results for the Yb-containing compound are shown in Figure 5) and by thermo-dependent X-ray diffraction (TDXD).

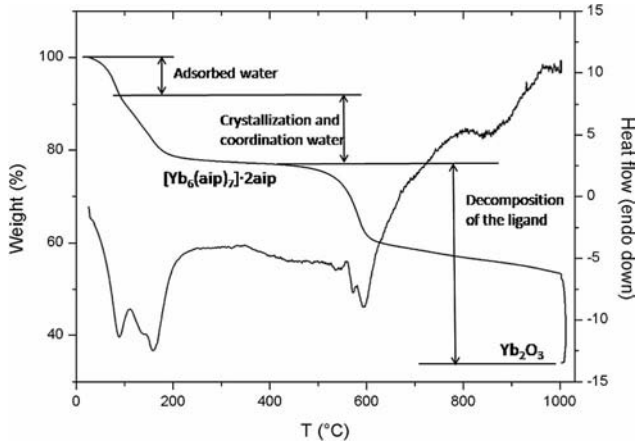

Figure 5. TG/TD analysis of compound $\{[Yb_6(aip)_7(H_2O)_{24}]\cdot 2(aip)\cdot 6H_2O\}_\infty$.

The TG/TD experiments confirm the water content determined by elemental analyses and by the crystal structure; the observed weight loss (16%) is in good agreement with that calculated from the crystal structure (17%). These mono-dimensional compounds show very low thermal stability. Actually, the water departure occurs between 75 and 150 °C and is accompanied by a collapse of the crystal structure. The resulting amorphous anhydrous compound remains unchanged until roughly 500 °C, after which time the aminoisophthalate ligand decomposes leading to the lanthanide oxide. Under a wet atmosphere, the amorphous anhydrous phase obtained between 150 and 500 °C revers-

ibly binds water leading to the initial hydrated compound. This demonstrates that below 500 °C, the molecular motif is not destroyed.

Family 2. $\{[Ln_2(aip)_2(H_2O)_{10}]\cdot(aip)\cdot 4H_2O\}_\infty$ in which Ln = La–Er (except Pm) or Y

The compounds that belong to Family 2 have the general chemical formula $\{[Ln_2(aip)_2(H_2O)_{10}]\cdot(aip)\cdot 4H_2O\}_\infty$ when Ln = La–Er (except Pm) or Y. They are isostructural and the crystal structure has been solved for the Eu-containing compound (Figure 6). The isostructurality of the other compounds of the family has been assumed on the basis of their X-ray diffraction diagrams and single-crystal X-ray diffraction data.

The crystal structure of $\{[Eu_2(aip)_2(H_2O)_{10}]\cdot(aip)\cdot 4H_2O\}_\infty$ is mono-dimensional and can be described as the juxtaposition of double-chain-like molecular motifs. Each motif consists of a sort of dimerization of two identical chains with the general chemical formula $[Ln_2(aip)_2(H_2O)_{10}]^{2+}$ spreading along the a + c direction (Figure 7). The two chains are strongly bound to each other by hydrogen bonds between coordinated water molecules and oxygen atoms belonging to carboxylate groups and by π-stacking interactions between aminoisophthalate ligands that belongs to adjacent chains (Figure 7): the mean distance between related oxygen atoms is about 2.7 Å whereas the mean distance between related C atoms is about 3.7 Å (Table 2).

Table 2. Selected contacts between the two adjacent chains that form a double-chain molecular motif.

Atom1	Atom2	Symmetry	Distance [Å]
O108	O11	–0.5 + *x*, 1 – *y*, –0.5 + *z*	2.633
O104	O22	0.5 + *x*, 1 – *y*, 0.5 + *z*	2.690
C28	C12	–0.5 + *x*, 1 – *y*, –0.5 + *z*	3.702
C27	C13	–0.5 + *x*, 1 – *y*, –0.5 + *z*	3.719
C26	C14	–0.5 + *x*, 1 – *y*, –0.5 + *z*	3.671
C16	C24	0.5 + *x*, 1 – *y*, 0.5 + *z*	3.682
C23	C17	–0.5 + *x*, 1 – *y*, –0.5 + *z*	3.699
C22	C18	–0.5 + *x*, 1 – *y*, –0.5 + *z*	3.678
O103	O24	0.5 + *x*, – *y*, 0.5 + *z*	2.729
O107	O14	–0.5 + *x*, – *y*, –0.5 + *z*	2.702
O102	O21	0.5 + *x*, – *y*, 0.5 + *z*	2.748
O105	O23	*x*, *y*, *z*	2.720
O12	O106	*x*, *y*, *z*	2.739

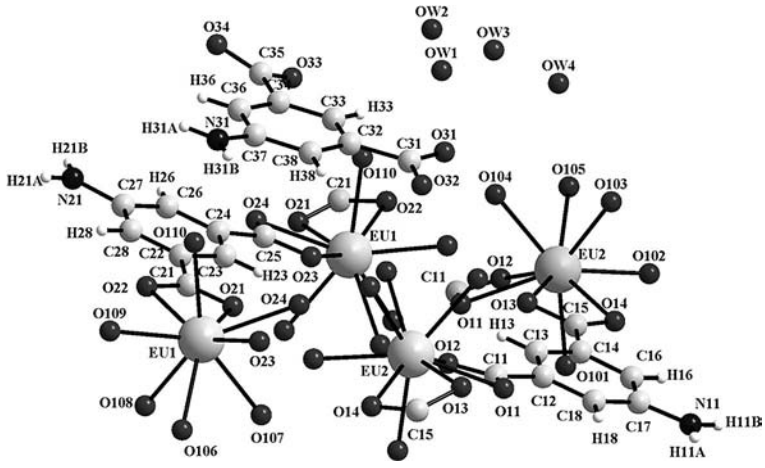

Figure 6. Projection view of an extended asymmetric unit of $\{[Eu_2(aip)_2(H_2O)_{10}]\cdot(aip)\cdot 4H_2O\}_\infty$.

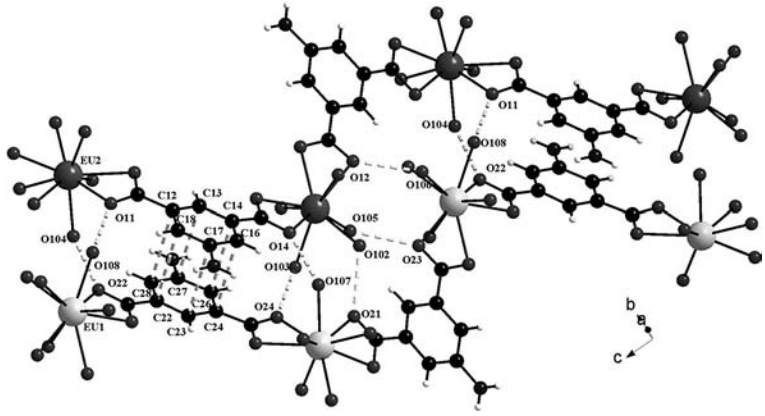

Figure 7. Projection view of two adjacent chains that form a double-chain molecular motif. Broken lines symbolize the shortest contacts between the two chains. The light grey spheres represent the Eu1 atoms whereas the dark grey represent the Eu2 atoms.

In the crystal structure, there are two crystallographically independent Eu atoms. Each one is involved in only one chain. Both Eu atoms are coordinated to nine oxygen atoms. In each case, four oxygen atoms belong to two bidentate carboxylate clips whereas the remaining five are from coordinated water molecules. The coordination polyhedrons can be described as slightly distorted tricapped trigonal prisms. The two crystallographically independent aminoisophthalate ligands are bound to Eu atoms in a bisbidentate manner.

The intrachain intermetallic distances are almost 10 Å (Eu1···Eu1 9.905 Å; Eu2···Eu2 9.894 Å). The closest contacts between Eu atoms belonging to the two different chains of the double-chain molecular motif are roughly equal to 6 Å (see Table 3); the second closest contacts are greater than 10 Å (Figure 8).

Table 3. Closest intermetallic contacts between adjacent chains.

Atom1	Atom2	Symmetry	Distance [Å]
Eu2	Eu1	*x*, *y*, *z*	6.392
Eu2	Eu1	0.5 + *x*, – *y*, 0.5 + *z*	6.008
Eu1	Eu2	–0.5 + *x*, 1 – *y*, –0.5 + *z*	5.986
Eu1	Eu2	–1 + *x*, *y*, –1 + *z*	11.458
Eu1	Eu1	1 + *x*, *y*, 1 + *z*	17.644
Eu1	Eu2	0.5 + *x*, 1 – *y*, 0.5 + *z*	16.023

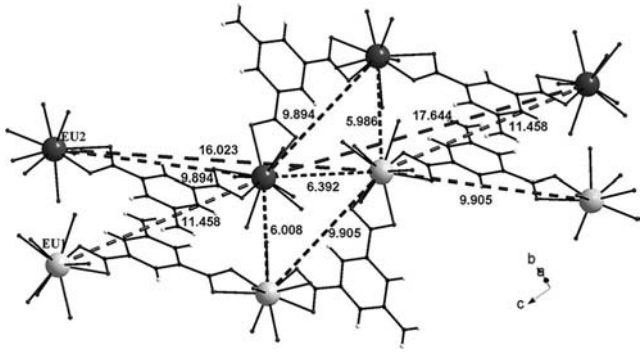

Figure 8. Closest intermetallic contact in a double-chain molecular motif.

Three crystallization water molecules and an uncoordinated aminoisophthalate ligand, insuring the electro-neutrality of the network, lie between the double-chain molecular motifs (Figure 9).

As shown in Figure 9, in the (a,c) plane, the double-chain molecular motifs are bound to each other by a complex network involving π-stacking[36] interactions and H-bonds. Selected distances of such intermolecular interactions are listed in Table 4.

Table 4. Selected intermolecular distances.

Atom1	Atom2	Symmetry	Distance [Å]
O33	O110	*x*, *y*, *z*	2.710
O101	OW1	1 + *x*, *y*, *z*	2.696
OW2	OW1	*x*, *y*, *z*	2.721
N31	OW2	0.5 + *x*, –*y*, 0.5 + *z*	2.956
OW3	O101	–1 + *x*, *y*, *z*	3.523
O107	O34	0.5 + *x*, –*y*, –0.5 + *z*	2.864
O32	O104	*x*, *y*, *z*	2.668
O31	O105	*x*, *y*, *z*	3.188
N31	N11	–0.5 + *x*, 1 – *y*, 0.5 + *z*	3.381
O34	OW4	*x*, –1 + *y*, *z*	2.848
O34	O108	–0.5 + *x*, –*y*, 0.5 + *z*	3.386
OW4	O32	–0.5 + *x*, 1 – *y*, –0.5 + *z*	2.759
OW4	N21	0.5 + *x*, 1 – *y*, 0.5 + *z*	3.004
C34	C26	0.5 + *x*, –*y*, 0.5 + *z*	3.876
C36	C27	0.5 + *x*, –*y*, 0.5 + *z*	3.852
C28	C37	–0.5 + *x*, –*y*, –0.5 + *z*	3.970
C38	C22	0.5 + *x*, –*y*, 0.5 + *z*	4.127
C32	C23	0.5 + *x*, –*y*, 0.5 + *z*	4.145
C33	C24	0.5 + *x*, –*y*, 0.5 + *z*	4.018

Each Eu atom of the complex is surrounded by ten other Eu atoms at distances less than 11 Å (Figure 10). As can be seen from Table 5 there is no significant difference between the Eu1 and the Eu2 surroundings.

The purity of the microcrystalline powder was determined by SEM measurements. All observations have unambiguously demonstrated the homogeneity of the samples (the measurements for the Tb-containing compound are shown in Figure 11). All the powder grains look like hedgehogs made of hexagonal plate-like crystallites. The grain size is rather homogeneous with a mean diameter of approximately 20 μm for all the samples.

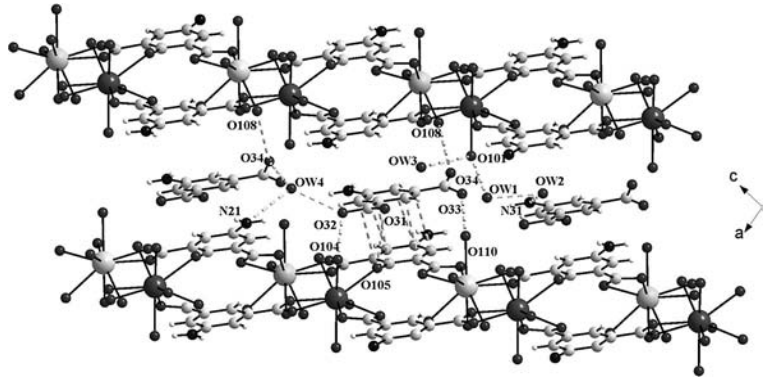

Figure 9. Projection view along the b axis of two double-chain molecular motifs. Broken lines symbolize π-stacking interactions and H-bonds.

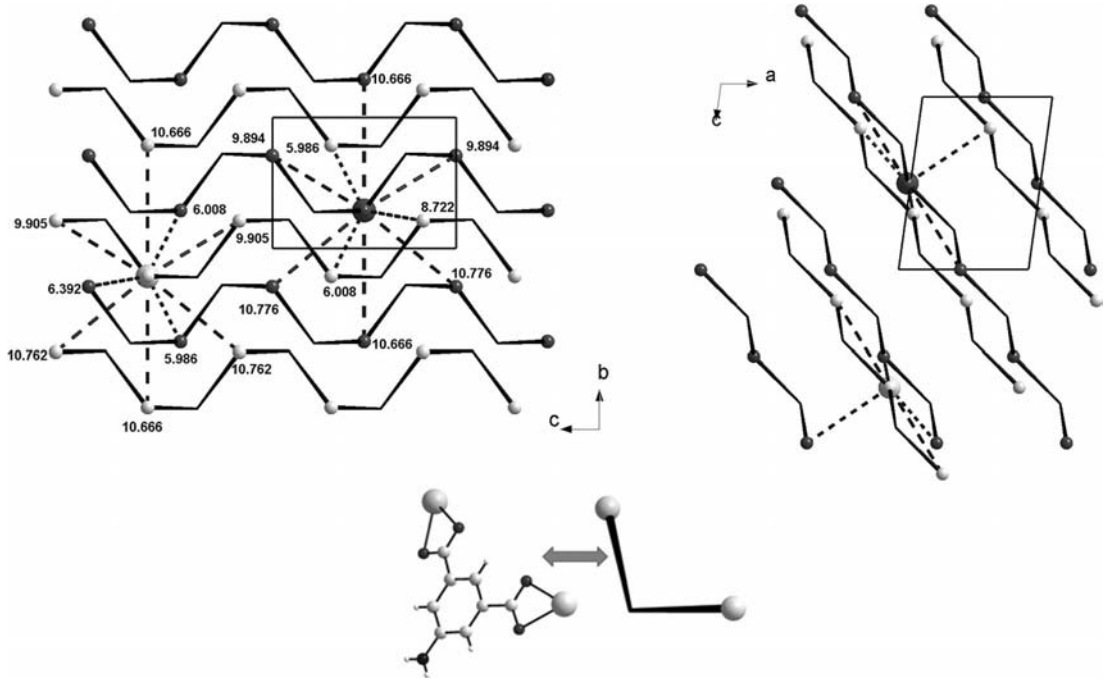

Figure 10. Schematic projection view along the a axis (left) and the b axis (right) of $\{[Eu_2(aip)_2(H_2O)_{10}]\cdot(aip)\cdot 4H_2O\}_\infty$. Light colored spheres symbolize Eu1 atoms whereas dark symbolize Eu2 atoms.

Table 5. Intermetallic distances smaller than 11 Å in $\{[Eu_2(aip)_2(H_2O)_{10}]\cdot(aip)\cdot 4H_2O\}_\infty$.

Atom1	Atom2	Symmetry	Distance [Å]
Eu2	Eu2	x, 1 + y, z	10.666
Eu2	Eu2	–0.5 + x, 1 – y, –0.5 + z	9.894
Eu2	Eu1	x, y, z	6.392
Eu2	Eu1	1 + x, y, z	8.722
Eu2	Eu1	0.5 + x, –y, 0.5 + z	6.008
Eu2	Eu2	0.5 + x, –y, 0.5 + z	10.776
Eu2	Eu2	0.5 + x, 1 – y, 0.5 + z	9.894
Eu2	Eu1	0.5 + x, 1 – y, 0.5 + z	5.986
Eu2	Eu2	–0.5 + x, –y, –0.5 + z	10.776
Eu2	Eu2	x, –1 + y, z	10.666
Eu1	Eu1	x, –1 + y, z	10.666
Eu1	Eu2	–0.5 + x, –y, –0.5 + z	6.008
Eu1	Eu1	–0.5 + x, –y, –0.5 + z	9.905
Eu1	Eu1	–0.5 + x, 1 – y, –0.5 + z	10.762
Eu1	Eu2	–0.5 + x, 1 – y, –0.5 + z	5.986
Eu1	Eu1	x, 1 + y, z	10.666
Eu1	Eu1	0.5 + x, 1 – y, 0.5 + z	10.762
Eu1	Eu2	x, y, z	6.392
Eu1	Eu2	–1 + x, y, z	8.722
Eu1	Eu1	0.5 + x, –y, 0.5 + z	9.905

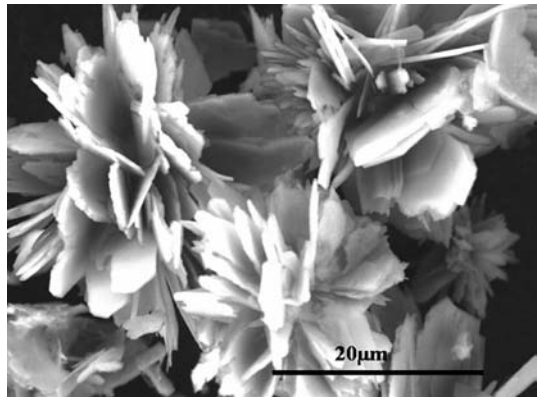

Figure 11. SEM measurement of a $\{[Tb_2(aip)_2(H_2O)_{10}]\cdot(aip)\cdot 4H_2O\}_\infty$ microcrystalline sample.

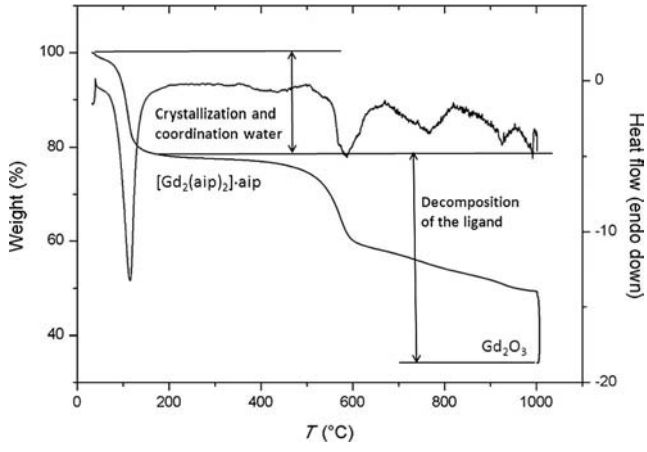

Figure 12. TG/TDA curves for $\{[Gd_2(aip)_2(H_2O)_{10}]\cdot(aip)\cdot 4H_2O\}_\infty$.

The thermal behaviors of the compounds belonging to Family 2 have been evaluated for the Gd-containing compound by coupled thermogravimetric and thermodifferential analyses (Figure 12) and by TDXD. These measurements first confirmed the hydration rate of the compound (seven water molecules per Gd atom). They also confirmed that the compound collapses upon dehydration leading to an amorphous anhydrous phase. This anhydrous phase re-

mains unchanged between 150 and 500 °C. The decomposition of the ligand then occurs leading, above 550 °C, to gadolinium oxide (Gd_2O_3). Actually, the integrity of the molecular skeleton is kept below 500 °C and the anhydrous compound reversibly binds water when exposed to wet atmosphere.

When exposed to UV radiation, some compounds belonging to Family 2 exhibit visible emission. A 3D scan of the luminescent properties of the Tb-containing compound (Figure 13) has been measured ($250 \leq \lambda_{exc} \leq 400$ and $450 \leq \lambda_{em} \leq 750$ nm). It clearly shows that the best excitation wavelength is 365 nm. This excitation wavelength was used for the following experiments. As can be noticed from Figure 13, the most luminescent compound is the Tb-containing one. The Sm-, the Tb-, and the Dy-containing compounds, respectively, emit purple, green, and yellow light. On the contrary, the red luminescence of the Eu-containing compound is very low. For all the other compounds, the observed blue light can be attributed to the blue ($x = 0.22$; $y = 0.32$) fluorescence of the ligand (Table 6). It is noticeable that the Dy- and the Sm-containing compounds present (x,y) colorimetric coordinates very near to ideal white-light coordinates (0.33, 0.33). This must be related to their low emission intensities.

The solid-state excitation and luminescent spectra have been recorded for the Sm-, the Eu-, the Gd-, the Dy-, and the Tb-containing compounds. All these compounds present a maximum in their excitation spectrum at 365 nm. This indicates that the aminoisophthalate ligand exhibits an antenna effect with respect to Sm^{III}, Tb^{III}, and Dy^{III} ions. All the luminescence decay rates are mono-exponential.

The Sm-containing compound exhibits three emission peaks at 560, 596, and 642 nm, which correspond to the $^4G_{5/2} \rightarrow {}^6H_{5/2}$, $^4G_{5/2} \rightarrow {}^6H_{7/2}$, and $^4G_{5/2} \rightarrow {}^6H_{9/2}$ transitions, respectively; the luminescent quantum yield is $\Phi = 0.19\%$ and the luminescent lifetime is 0.011 ms (Figure 14). The Tb-containing compound exhibits four intense emission peaks (Figure 14) at 490, 545, 590, and 620 nm, which correspond to the $^3D_4 \rightarrow {}^7F_6$, $^3D_4 \rightarrow {}^7F_5$, $^3D_4 \rightarrow {}^7F_4$, and $^3D_4 \rightarrow {}^7F_3$ transitions, respectively. The luminescent lifetime is 0.471 ms and the quantum yield is $\Phi = 32\%$. Despite some short intermetallic distances (see Tables 3 and 5), this

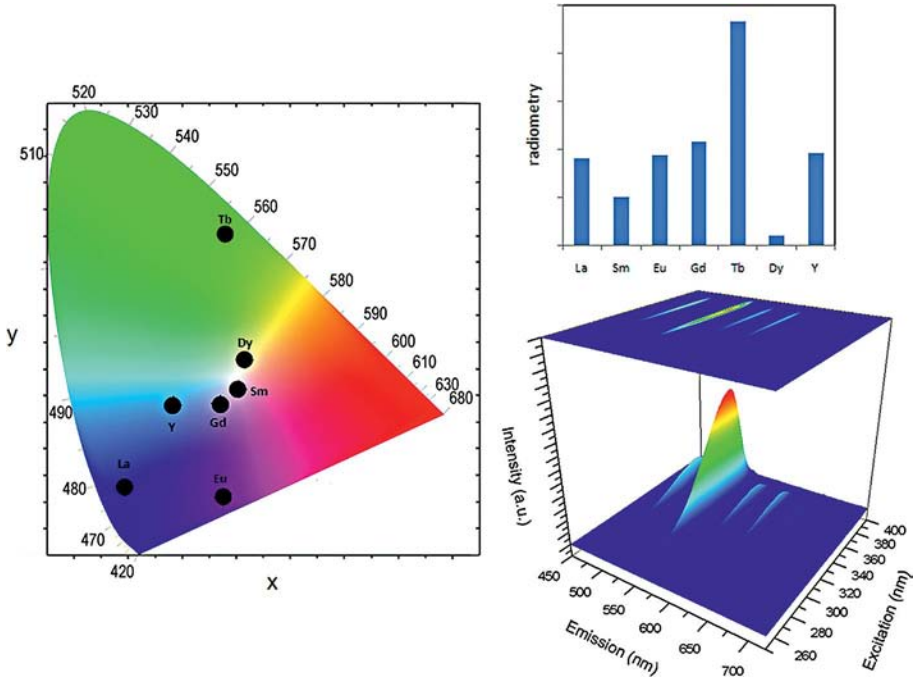

Figure 13. Left: Colorimetric data ($\lambda_{exc} = 365$ nm) for compounds $\{[Ln_2(aip)_2(H_2O)_{10}]\cdot(aip)\cdot 4H_2O\}_\infty$ in which Ln = La–Sm, Eu, Gd, Tb, Dy, Y. Top right: Radiometric measurements ($\lambda_{exc} = 365$ nm) given in arbitrary units. Bottom right: 3D representation of the luminescent properties of the Tb-containing compound.

Table 6. Colorimetric data for compounds $\{[Ln_2(aip)_2(H_2O)_{10}]\cdot(aip)\cdot 4H_2O\}_\infty$ in which Ln = La–Sm, Eu, Gd, Tb, Dy, Y (*: the values are expressed in arbitrary units and represent the luminous flux weighted by the spectral response of the human eye).

Ln	x	y	Photometry*	Ln	x	y	Photometry*
La	0.144	0.13	46	Gd	0.32	0.28	68
Sm	0.36	0.31	205	Tb	0.33	0.608	33668
Eu	0.33	0.11	7	Dy	0.37	0.36	99
Y	0.24	0.28	133				

quantum yield is rather high. The Dy-containing compound exhibits two emission peaks (Figure 14) at 480 and 575 nm, which correspond to the $^7F_{9/2} \rightarrow {}^6H_{15/2}$ and $^7F_{9/2} \rightarrow {}^6H_{13/2}$ transitions. The luminescent quantum yield and lifetimes are $\Phi = 0.64\%$ and 0.005 ms. Surprisingly, the Eu-containing compound exhibits almost no emission upon irradiation. This indicates a low ligand-to-metal energy transfer with respect with the Eu^{III} ion. This was unexpected because the emission states of Eu^{III} ($^5D_0$ state, 17300 cm^{-1}) and of Sm^{III} ($^4G^{5/2}$ state, 17700 cm^{-1}) are similar. On the other hand, simple amino groups are known to quench the luminescence of Eu^{III} complexes by a photoinduced electron transfer (PET) process.[37] Although we have no experimental evidence for the moment, this PET process could explain why no luminescence was observed for the Eu-containing compound.

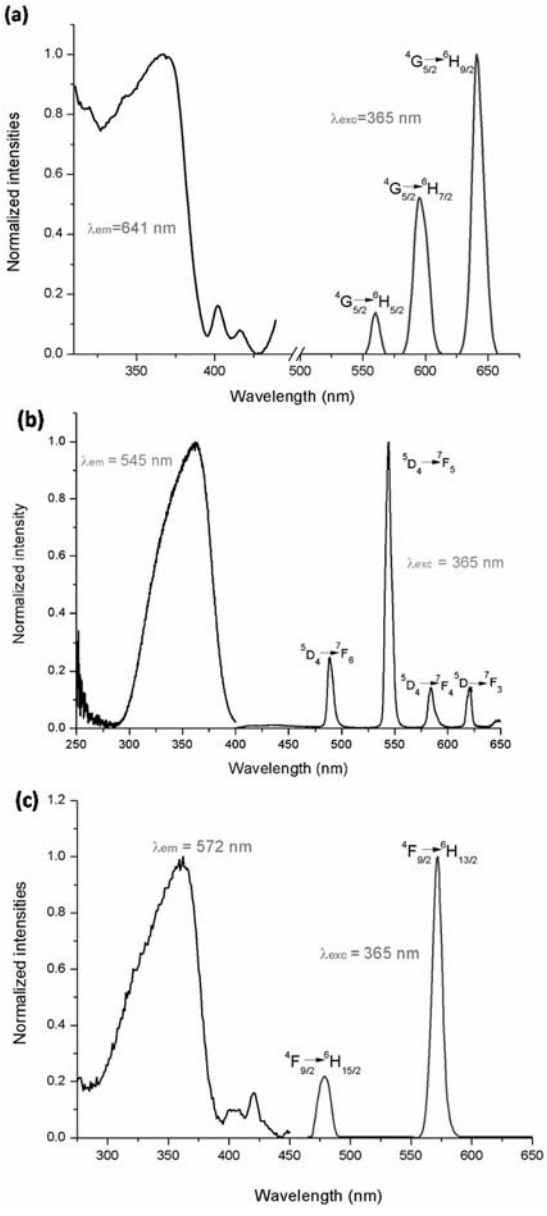

Figure 14. Excitation and luminescent spectra of $\{[Sm_2(aip)_2(H_2O)_{10}]\cdot(aip)\cdot 4H_2O\}_\infty$ (a), $\{[Tb_2(aip)_2(H_2O)_{10}]\cdot(aip)\cdot 4H_2O\}_\infty$ (b), and $\{[Dy_2(aip)_2(H_2O)_{10}]\cdot(aip)\cdot 4H_2O\}_\infty$ (c).

Conclusion

We have reported here on two new families of lanthanide-containing coordination polymers obtained through green synthetic methods. Some compounds belonging to Family 2 exhibit some rather intense luminescence under UV irradiation.

Recently our group has reported a family of isostructural hetero-polynuclear lanthanide-based coordination polymers exhibiting tunable luminescent properties versus the ratio between the different involved lanthanide ions.[38]

According to this study, compounds belonging to Family 2 seem to constitute a rather promising system for the design of such a family of hetero-polynuclear compounds with tunable luminescent properties. Actually, their crystal structure can accommodate most of the lanthanide ions (from La to Er plus Y) and three out of the eleven homonuclear compounds exhibit rather strong luminescence upon UV irradiation. To verify this assumption, we have synthesized the hetero-binuclear compound $\{[SmTb(aip)_2(H_2O)_{10}]\cdot(aip)\cdot 4H_2O\}_\infty$ and compared its luminescent properties to those of a microcrystalline mixture (50:50) of $\{[Tb_2(aip)_2(H_2O)_{10}]\cdot(aip)\cdot 4H_2O\}_\infty$ and $\{[Sm_2(aip)_2(H_2O)_{10}]\cdot(aip)\cdot 4H_2O\}_\infty$. The results of these experiments (Figure 15) unambiguously demonstrate that both systems exhibit different luminescent properties (colorimetric coordinates of the hetero-binuclear compounds are identical to those of the Tb-containing mononuclear compound).

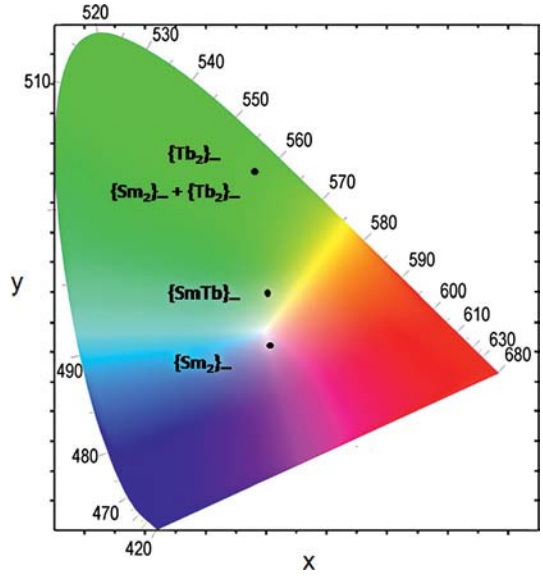

Figure 15. Colorimetric data under UV irradiation ($\lambda_{exc.} = 365$ nm) for compounds $\{[Tb_2(aip)_2(H_2O)_{10}]\cdot(aip)\cdot 4H_2O\}_\infty$ ($\{Tb\}_\infty$), $\{[Sm_2(aip)_2(H_2O)_{10}]\cdot(aip)\cdot 4H_2O\}_\infty$ ($\{Sm\}_\infty$), $\{[SmTb(aip)_2(H_2O)_{10}]\cdot(aip)\cdot 4H_2O\}_\infty$ ($\{SmTb\}_\infty$), and for a 50%/50% mixture of $\{[Tb_2(aip)_2(H_2O)_{10}]\cdot(aip)\cdot 4H_2O\}_\infty$ and $\{[Sm_2(aip)_2(H_2O)_{10}]\cdot(aip)\cdot 4H_2O\}_\infty$ ($\{Sm\}_\infty + \{Tb\}_\infty$).

We are convinced that hetero-polynuclear lanthanide-based coordination polymers could be of great interest as far as luminescent devices are concerned. Therefore, we have undertaken the detailed study of the system $\{[Ln'_xLn_{2-x}(aip)_2(H_2O)_{10}]\cdot(aip)\cdot 4H_2O\}_\infty$ in which Ln = La–Er or Y (except Pm) and $0 \leq x \leq 2$.

Experimental Section

Synthesis of the Microcrystalline Powders: 5-amino-1,3-benzene dicarboxylic acid (H_2aip) was purchased from Acros Organics and used without further purification. The disodium aminoisophthalate salt was prepared by the addition of two equivalents of sodium hydroxide to a suspension of aminoisophthalic acid in deionized water. The obtained clear solution was then evaporated to dryness. The resulting solid was suspended in a small amount of ethanol. The mixture was stirred and refluxed for 1 h. Upon addition of ethoxyethane, precipitation occurred. After filtration and drying, a white powder of the disodium salt of 5-amino-1,3-benzene dicarboxylic acid was collected in 90% yield. $C_8H_5NNa_2O_4$ (225.11): calcd. C 42.68, H 2.24, N 6.22, Na 20.42, O 28.43; found C 42.55, H 2.00, N 6.41, Na 20.42, O 28.71.

Hydrated lanthanide chlorides were prepared from the corresponding oxides according to literature methods.[39] Lanthanide oxides were purchased from STREM Chemicals and used without further purification.

Microcrystalline powders of the coordination polymers were obtained by mixing stoichiometric amounts of lanthanide chloride in water with the disodium salt of aminoisophthalic acid. Precipitation immediately occurred. The precipitates were removed by filtration and dried in air. The yields of the reactions were close to 90%. Two families of isostructural coordination polymers were obtained depending on the involved lanthanide ion. The obtained microcrystalline powders have been assumed to be isostructural, on the basis of their X-ray powder diffraction diagrams (Figures 16 and 17). The results of the elemental analyses are listed in Tables 7 and 8.

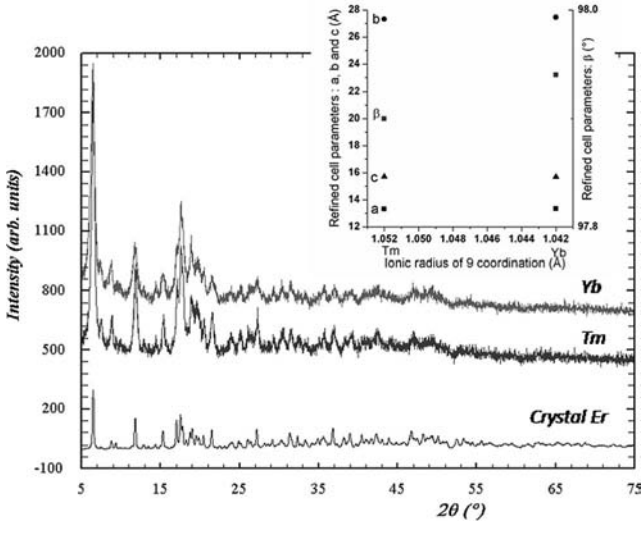

Figure 16. Experimental X-ray diffraction diagrams of the microcrystalline powders obtained for Ln = Tm–Yb (Family 1) and simulated X-ray diffraction pattern of $\{[Er_6(aip)_7(H_2O)_{24}]\cdot 2(aip)\cdot 6H_2O\}_\infty$. The inset shows the fitted cell parameters versus the ionic radius of the involved lanthanide ion. Ionic radii are for nine-coordinate ions.[40]

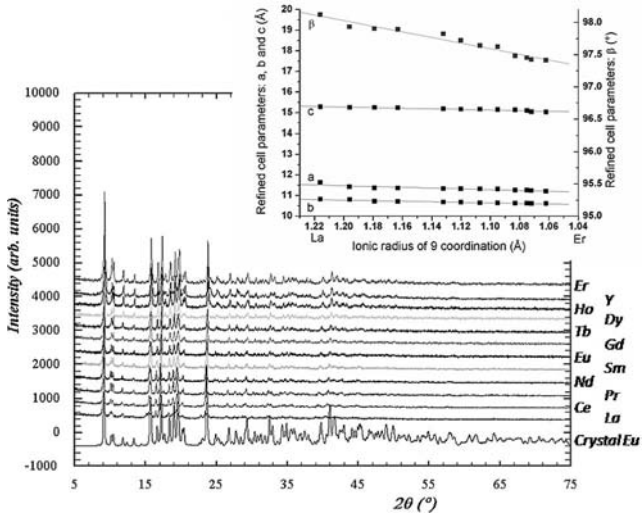

Figure 17. Experimental X-ray diffraction diagrams of the microcrystalline powders obtained for Ln = La–Er or Y (except Pm; Family 2) and simulated X-ray diffraction pattern of $\{[Eu_2(aip)_2(H_2O)_{10}]\cdot(aip)\cdot 4H_2O\}_\infty$. The inset shows the fitted cell parameters versus the ionic radius of the involved lanthanide ion. Ionic radii are for nine-coordinate ions.[40]

FT-IR spectra show the expected strong characteristic absorptions for the symmetric and asymmetric vibrations of benzene-dicarboxylate ligands (1650–1550 and 1420–1335 cm^{-1}). They show no absorption band of any protonated carboxylic group (1715–1680 cm^{-1}).

Synthesis of the Single Crystals: Tetraethyl-orthosilicate (TEOS), tetramethyl-orthosilicate (TMOS), and agarose were purchased from Acros Organics and gelified according to established procedures.[18,41–42] Dilute solutions of Ln^{III} chloride (0.1 mol L^{-1}) and disodium aminoisophthalate (0.1 mol L^{-1}) were allowed to slowly diffuse through the gel media in a U-shaped tube. After a few weeks, single crystals were obtained. Alternatively, single crystals could be obtained by the slow diffusion through water in an H-shaped tube. Details of the different crystal growth conditions are listed in Table 9.

FT-IR Measurements: FT-IR measurements have been performed on KBr pellets between 400 and 4000 cm^{-1} using a Perkin–Elmer Paragon 1000 PC spectrometer. All compounds exhibit similar IR spectra: $\tilde{\nu}$ = 3336 (vs), 1607 (s), 1532 (vs), 1451 (s), 1396 (vs), 998 (w), 777 (w), 724 (w).

X-Ray Powder Diffraction: The powder diffraction diagrams were collected using a Panalytical X'Pert Pro diffractometer with an X'Celerator detector. The typical recording conditions were 40 kV and 40 mA for Cu-K_α (λ = 1.542 Å); the diagrams were recorded in θ/θ mode over 60 min between 5 and 75° (8378 measurements) with a step size of 0.0084° and a scan time of 50 s. The calculated patterns were produced using the Powdercell and WinPLOTR software programs.[43–45] For Pattern indexing, the extractions of the peak positions were carried out using the WinPLOTR software. The pattern indexing was performed by the program McMaille[46] and the refinement of the unit cell parameters by means of the Chekcell program, which is a modified version of Cellref from CRYSFIRE suite.[47]

Table 7. Chemical analyses for $\{[Ln_6(aip)_7(H_2O)_{24}]\cdot 2(aip)\cdot 6H_2O\}_\infty$ in which Ln = Tm–Yb.

Ln	MW [g mol^{-1}]	Microanalysis, calcd. (found) Ln [%]	O [%]	C [%]	H [%]	N [%]
Tm	3166.25	32.01 (31.51)	33.35 (33.55)	27.31 (27.49)	3.34 (3.43)	3.98 (4.08)
Yb	3190.90	32.54 (32.34)	33.09 (33.29)	27.10 (27.02)	3.32 (3.38)	3.95 (4.00)

Table 8. Chemical analysis for $\{[Ln_2(aip)_2(H_2O)_{10}]\cdot(aip)\cdot 4H_2O\}_\infty$ in which Ln = La – Er or Y (except Pm).

Ln	MW [g mol^{-1}]	Microanalysis, calcd. (found) Ln [%]	O [%]	C [%]	H [%]	N [%]
La	1067.42	26.03 (26.21)	38.97 (38.91)	27.00 (27.21)	4.16 (4.07)	3.95 (3.75)
Ce	1069.85	26.19 (26.01)	38.88 (39.08)	26.95 (26.85)	4.05 (4.14)	3.93 (3.99)
Pr	1071.43	26.30 (26.10)	38.88 (39.08)	26.94 (26.91)	4.05 (4.25)	3.92 (4.12)
Nd	1078.09	26.76 (26.76)	38.59 (38.39)	26.94 (26.92)	4.02 (4.18)	3.89 (3.71)
Sm	1090.33	27.58 (27.51)	38.15 (38.01)	26.44 (26.73)	3.97 (4.01)	3.92 (3.99)
Eu	1093.54	27.79 (27.89)	38.04 (38.02)	26.36 (26.30)	3.96 (4.06)	3.84 (3.71)
Gd	1104.11	28.48 (28.32)	37.68 (37.89)	26.11 (26.09)	3.93 (3.97)	3.81 (3.71)
Tb	1107.46	28.70 (28.95)	37.56 (37.54)	26.03 (26.04)	3.91 (3.73)	3.79 (3.89)
Dy	1114.61	29.16 (29.19)	37.32 (37.45)	25.86 (25.64)	3.88 (3.90)	3.76 (3.81)
Ho	1119.47	29.47 (29.48)	37.16 (37.01)	25.75 (25.71)	3.87 (3.96)	3.75 (3.80)
Er	1124.13	29.76 (29.96)	37.01 (36.91)	25.64 (25.53)	3.86 (4.01)	3.74 (3.63)
Y	967.42	18.38 (18.40)	42.99 (43.28)	29.80 (29.71)	4.48 (4.42)	4.34 (4.23)

Table 9. Summary of the crystal growth conditions.

Diffusion through agarose gel in a U-shaped tube.	
Gel density (in weight percent): 0.1	$\{[La_2(aip)_2(H_2O)_{10}]\cdot(aip)\cdot 4H_2O\}_\infty$
Diffusion through TEOS gel in a U-shaped tube.	
Gel density (in volumic percent): 7.5	$\{[Ln_2(aip)_2(H_2O)_{10}]\cdot(aip)\cdot 4H_2O\}_\infty$ (Ln = Nd, Eu, Tb, Y, Er)
Diffusion through TMOS gel in a U-shaped tube.	
Gel density (in volumic percent): 7.5	$\{[Ln_2(aip)_2(H_2O)_{10}]\cdot(aip)\cdot 4H_2O\}_\infty$ (Ln = Ce–Gd, Dy–Er, Y)
Diffusion through water in a H-shaped tube	
	$\{[Ln_6(aip)_7(H_2O)_{24}]\cdot 2(aip)\cdot 6H_2O\}_\infty$ (Ln = Er–Yb) $\{[Ln_2(aip)_2(H_2O)_{10}]\cdot(aip)\cdot 4H_2O\}_\infty$ (Ln = Ce–Ho, Er)

Thermal dependent X-ray diffraction experiments were performed on a Panalytical X'Pert Pro diffractometer with an X'Celerator detector using Cu-$K_{\alpha 1}$ radiation in the range 5–75° in 2θ. The heating of the samples (from room temperature to 1000 °C) was performed using an Anton Paar HTK 1200 furnace under a nitrogen atmosphere.

The identification of the phases based on their X-ray diffraction diagrams has been done by using the Highscore Software[48] with a JCPDS version PDF2/2000 (sets 1–50 and 70–88) database.

Thermal Analysis: Thermo-gravimetric and thermo-differential analyses were performed in platinum crucibles under a nitrogen atmosphere between room temperature and 1000 °C with a heating rate of 5 °C min^{-1} using a Perkin–Elmer Pyris-Diamond thermal analyzer. At the end of the experiments, the compounds were maintained for 1 h at 1000 °C under an ambient atmosphere to complete the combustion.

Single Crystal X-ray Diffraction Data: All crystals were sealed in glass capillaries for X-ray single crystal data collection to avoid potential dehydration. Needle-like single crystals of Family 1 were mounted on an APEXII AXS-Bruker diffractometer with Mo-K_α radiation (λ = 0.71073 Å). Hexagonal plate-like single crystals of Family 2 (Figure 18) were mounted on a Nonius Kappa CCD diffractometer with Mo-K_α radiation (λ = 0.71073 Å). The crystal data collections were performed at room temperature.

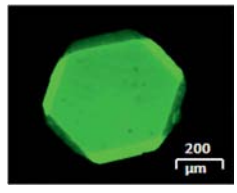

Figure 18. Hexagonal plate-like single crystal of $\{[Tb_2(aip)_2(H_2O)_{10}]\cdot(aip)\cdot 4H_2O\}_\infty$ under UV irradiation (λ_{exc} = 365 nm).

Absorption corrections were performed using the facilities[49–52] included in the WinGX program suite.[51]

The structure was solved by direct methods using the SIR97 program,[53] and then refined with full-matrix least-square methods based on F^2 (SHELX-97)[50] with the aid of WINGX program.[51] Crystal and final structure refinement data of $\{[Eu_2(aip)_2(H_2O)_{10}]\cdot(aip)\cdot 4H_2O\}_\infty$ are listed in Table 10.

For Family 1, the contribution of the disordered solvents to the calculated structure factors was estimated following the BYPASS algorithm,[53] implemented as the SQUEEZE option in PLATON.[54] A new data set, free of solvent contribution, was then used in the final refinement.

All non-hydrogen atoms were refined anisotropically using the SHELXL program.[50] Hydrogen atoms bound to the organic li-

Table 10. Crystal and final structure refinement for $\{[Er_6(aip)_7(H_2O)_{24}]\cdot 2(aip)\cdot 6H_2O\}_\infty$ (**1**) and $\{[Eu_2(aip)_2(H_2O)_{10}]\cdot(aip)\cdot 4H_2O\}_\infty$ (**2**).

	1	**2**
Chemical formula	$Er_3C_{36}O_{33}N_{4.5}H_{52.5}$	$Eu_2C_{24}O_{26}N_3H_{43}$
System	monoclinic	monoclinic
a [Å]	13.344(5)	11.3427(2)
b [Å]	27.333(5)	10.6663(1)
c [Å]	15.719(5)	15.1639(3)
β [°]	97.785(5)	97.8998(9)
V [Å^3]	5680(3)	1817.19(5)
Z	4	2
Formula weight [g mol^{-1}]	1578.10	1093.53
Space group (No.)	$P1\ 21/n\ 1$ (14)	$P1\ n\ 1$ (7)
$D_{calcd.}$ [g cm^{-3}]	1.845	1.999
μ [mm^{-1}]	4.486	3.523
R [%]	4.99	4.38
R_W [%]	19.82	11.13

gand were localized at ideal positions. Hydrogen atoms of water molecules have not been localized. Crystal and final structure refinement data of $\{[Er_6(aip)_7(H_2O)_{24}]\cdot 2(aip)\cdot 6H_2O\}_\infty$ are listed in Table 10.

CCDC-802306 (for $\{[Er_6(aip)_7(H_2O)_{24}]\cdot 2(aip)\cdot 6H_2O\}_\infty$) and -802305 (for $\{[Eu_2(aip)_2(H_2O)_{10}]\cdot(aip)\cdot 4H_2O\}_\infty$) contain the supplementary crystallographic data for this paper. These data can be obtained free of charge from The Cambridge Crystallographic Data Centre via www.ccdc.cam.ac.uk/data_request/cif.

Scanning Electron Microscopy – Energy-Dispersive Spectroscopy (SEM–EDS Analysis): All SEM observations and EDS measurements were carried out with a Hitachi TM-1000, Tabletop Microscope version 02.11 (Hitachi High-Technologies, Corporation Tokyo Japan) with EDS analysis system (SwiftED-TM, Oxford Instruments Link INCA). The detector is a Silicon drift detector, with an energy resolution of 165 eV that allows us to detect the elements from Na to U. With the software SwiftED-TM, qualitative and quantitative analyses can be realized. All the samples have been observed by means of an electron beam accelerated at 15 kV under high vacuum. The samples were assembled on carbon discs, stuck on an aluminum stub fixed at 7 mm from EDX beam, with an angle of measurement of 22°.

Solid State Luminescence Measurements: Solid-state emission spectra were measured on a Horiba Jobin–Yvon Fluorolog III fluorescence spectrometer with a pulse Xe lamp. Slit widths for excitation and emission were 2 nm for the Tb-containing compound and 5 nm for the Sm- and the Dy-containing compounds.

Luminescence spectra were all recorded at room temperature between 450 and 800 nm under identical operating conditions without turning the lamp off to ensure a valid comparison between the emission spectra. Reproducibility of the measurements was carefully checked by performing the experiments several times. The data were collected at every nm with an integration time of 100 ms for each step. The quantum yield measurements were performed using a Jobin–Yvon integrating sphere [$\Phi = (E_c - E_a)/(L_a - L_c)$ with E_c: emission spectrum of the sample, E_a: "blank" emission spectrum, L_a: "blank" absorption and L_c: sample absorption around excitation wavelength].

3D luminescent spectra were measured varying the excitation wavelength between 250 and 400 nm.

Colorimetric Measurements: The CIE (Commission Internationale de l'Eclairage) (x,y) emission color coordinates[55–56] were obtained using a MSU-003 colorimeter (Majantys) with the PhotonProbe 1.6.0 Software (Majantys). The excitation wavenumber was 365 nm. As a reference, the emission color coordinates of the standard red phosphor Gd_2O_2S:Eu (x = 0.667, y = 0.330) and green phosphor Gd_2O_2S:Tb (x = 0.328, y = 0.537) from Phosphor Technology were measured.

Acknowledgments

The China Scholarship Council PhD Program, Co-operation program with the French UT & INSA is acknowledged for financial support. The Center of Diffraction X of the University of Rennes 1 (CDIFX) is acknowledged for single-crystal X-ray diffraction data collections.

[1] F. Serpaggi, G. Férey, *Microporous Mesoporous Mater.* **1999**, *32*, 311.
[2] C. Serre, F. Millange, S. Surblé, G. Férey, *Angew. Chem.* **2004**, *116*, 6445; *Angew. Chem. Int. Ed.* **2004**, *43*, 6285.
[3] S. Surblé, C. Serre, F. Millange, G. Férey, *Solid State Sci.* **2006**, *8*, 413.
[4] F. Pellé, S. Surblé, C. Serre, F. Millange, G. Férey, *J. Lumin.* **2007**, *122–123*, 492.
[5] T. M. Reineke, M. Eddaoudi, M. O'Keeffe, O. M. Yaghi, *Angew. Chem.* **1999**, *111*, 2712; *Angew. Chem. Int. Ed.* **1999**, *38*, 2590.
[6] J. L. C. Rowsell, O. M. Yaghi, *Microporous Mesoporous Mater.* **2004**, *73*, 3.
[7] H. Deng, C. J. Doonan, H. Furukawa, R. B. Ferreira, J. Towne, C. B. Knobler, B. Wang, O. M. Yaghi, *Science* **2010**, *327*, 846.
[8] C. Janiak, *Dalton Trans.* **2003**, 2781.
[9] C. Janiak, J. K. Vieth, *New J. Chem.* **2010**, *34*, 2366.
[10] C. Daiguebonne, N. Kerbellec, K. Bernot, Y. Gérault, A. Deluzet, O. Guillou, *Inorg. Chem.* **2006**, *45*, 5399.
[11] N. Kerbellec, C. Daiguebonne, K. Bernot, O. Guillou, X. Le Guillou, *J. Alloys Compd.* **2008**, *451*, 377.
[12] D. Kustaryono, N. Kerbellec, G. Calvez, C. Daiguebonne, O. Guillou, *Cryst. Growth Des.* **2010**, *10*, 775.
[13] Y. Luo, G. Calvez, S. Freslon, C. Daiguebonne, T. Roisnel, O. Guillou, *Inorg. Chim. Acta* **2010**, *368*, 170.
[14] C. Daiguebonne, N. Kerbellec, O. Guillou, J. C. G. Bünzli, F. Gumy, L. Catala, T. Mallah, N. Audebrand, Y. Gérault, K. Bernot, G. Calvez, *Inorg. Chem.* **2008**, *47*, 3700.
[15] C. Daiguebonne, N. Kerbellec, Y. Gérault, O. Guillou, *J. Alloys Compd.* **2008**, *451*, 372.
[16] V. Haquin, F. Gumy, C. Daiguebonne, J. C. G. Bünzli, O. Guillou, *Eur. J. Inorg. Chem.* **2009**, 4491.
[17] P. T. Anastas, J. C. Warner, *Green Chemistry: Theory and Practice*, Oxford University Press Inc., New York, **2000**.
[18] C. Daiguebonne, A. Deluzet, M. Camara, K. Boubekeur, N. Audebrand, Y. Gérault, C. Baux, O. Guillou, *Cryst. Growth Des.* **2003**, *3*, 1015.
[19] O. Guillou, C. Daiguebonne, in: *Handbook on the Physics and Chemistry of Rare Earths*, vol. 34 (Eds.: K. A. Gschneider, J. C. G. Bünzli, V. K. Pecharsky), Elsevier, Amsterdam, **2005**, pp. 359.
[20] T. M. Reneike, M. Eddaoudi, M. Fehr, D. Kelley, O. M. Yaghi, *J. Am. Chem. Soc.* **1999**, *121*, 1651.
[21] L. Pan, E. B. Woodlock, X. Wang, *Inorg. Chem.* **2000**, *39*, 4174.
[22] Y. Wan, L. Jin, K. Wan, L. Zhang, X. J. Zheng, S. Lu, *New J. Chem.* **2002**, *26*, 1590.
[23] Y. Zhou, F. Jiang, Y. Xu, R. Cao, M. Hong, *J. Mol. Struct.* **2004**, *691*, 191.
[24] Y. Qu, Y. Ke, S. Lu, R. Fan, G. Pan, J. Li, in: *Journal of Molecular Structure*, vol. 734, **2005**, p. 7.
[25] H. J. Kim, D. Min, H. S. Hoe, S. W. Lee, *J. Korean Chem. Soc.* **2001**, *45*, 507.
[26] L. P. Zhang, Y. H. Wan, L. P. Jin, *Polyhedron* **2003**, *22*, 981.

[27] Y. Qiu, H. Deng, S. Yang, J. Mou, C. Daiguebonne, N. Kerbellec, O. Guillou, S. R. Batten, *Inorg. Chem.* **2009**, *48*, 3976.
[28] Y. Wu, N. Zheng, R. Yang, H. Xu, E. Ye, *J. Mol. Struct.* **2002**, *610*, 181.
[29] H. T. Xu, N. W. Zheng, X. L. Jin, R. Y. Yang, Z. Q. Li, *J. Mol. Struct.* **2003**, *646*, 197.
[30] H. T. Xu, N. W. Zheng, X. L. Jin, R. Y. Yang, Z. Q. Li, *J. Mol. Struct.* **2003**, *654*, 183.
[31] X. Haitao, Z. Nengwu, J. Xianglin, Y. Ruyi, W. Yonggang, Y. Enyi, L. Zhengquan, *J. Mol. Struct.* **2003**, *655*, 339.
[32] Z. Rzaczynska, M. Wozniak, W. Wolodkiewicz, A. Ostasz, S. Pikus, *J. Therm. Anal. Calorim.* **2008**, *91*, 951.
[33] C. B. Liu, X. J. Zheng, L. P. Jin, *J. Chem. Crystallogr.* **2006**, *36*, 199.
[34] X. Y. Chen, B. Zhao, W. Shi, J. Xia, P. Cheng, D. Z. Liao, S. P. Yan, Z. H. Jiang, *Chem. Mater.* **2005**, *17*, 2866.
[35] B. Yan, Y. Huang, M. Shao, *Solid State Sci.* **2008**, *10*, 90.
[36] C. Janiak, *J. Chem. Soc., Dalton Trans.* **2000**, 3885.
[37] C. Galaup, J.-M. Couchet, S. Bedel, P. Tisnès, C. Picard, *Eur. J. Org. Chem.* **2005**, *70*, 2274.
[38] N. Kerbellec, D. Kustaryono, V. Haquin, M. Etienne, C. Daiguebonne, O. Guillou, *Inorg. Chem.* **2009**, *48*, 2837.
[39] J. F. Desreux, in: *Lanthanide Probes in Life, Chemical and Earth Sciences* (Eds.: G. R. Choppin, J. C. G. Bünzli), Elsevier, Amsterdam, **1989**, p. 43.
[40] Shannon, *Acta Crystallogr., Sect. A* **1976**, *32*, 751.
[41] H. K. Henisch, R. Rustum, *Crystal Growth in Gels*, The Pennsylvania State University Press, **1970**.
[42] H. K. Henisch, *Crystals in Gels and Liesegang Rings*, Cambridge University Press, Cambridge, **1988**.
[43] W. Kraus, G. Nolze, *J. Appl. Crystallogr.* **1996**, *29*, 301.
[44] T. Roisnel, J. Rodriguez-Carjaval, *Materials Science Forum, Proceedings of the Seventh European Powder Diffraction Conference (EPDIC 7)* **2000**, 118.
[45] T. Roisnel, J. Rodriguez-Carjaval, *Mater. Sci. Forum* **2001**, *118*, 378.
[46] A. Le Bail, *Powder Diffr.* **2004**, *19*, 249.
[47] R. Shinley, in: *The CRYSFIRE system for automatic powder indexing*.
[48] N. V. Koninklijke Philips Electronics, *X'Pert Highscore*, Philips Analytical B. V., Almelo, The Nederlands, **2001**.
[49] A. Altomare, M. C. Burla, M. Camalli, B. Carrozzini, G. Cascarano, C. Giacovazzo, A. Guagliardi, A. G. G. Moliterni, G. Polidori, A. C. Rizzi, *J. Appl. Crystallogr.* **1999**, *32*, 339.
[50] G. M. Sheldrick, T. R. Schneider, *Macromol. Crystallography Part B* **1997**, 319.
[51] L. J. Farrugia, *J. Appl. Crystallogr.* **1999**, *32*, 837.
[52] P. Sluis, A. L. Spek, *Acta Crystallogr., Sect. A* **1990**, *46*, 194.
[53] A. Altomare, M. C. Burla, M. Camalli, G. Cascarano, C. Giacovazzo, A. Guagliardi, A. G. G. Moliterni, G. Polidori, R. Spagna, *J. Appl. Crystallogr.* **1999**, *32*, 115.
[54] A. L. Spek, *Acta Crystallogr., Sect. A* **1990**, *46*, C34.
[55] G. Wyszecki, in: *Handbook of Optics* (Eds.: W. G. Driscoll, W. Vaughan), Mac Graw-Hill Book Company, New York, **1978**, pp. 1.
[56] Color measurements: 2°, CIE 1931, step 5 nm, under 365 nm UV light.

$$X = k \times \int_{380nm}^{780nm} I_\lambda \times x_\lambda,$$

$$Y = k \times \int_{380nm}^{780nm} I_\lambda \times y_\lambda \text{ and}$$

$$Z = k \times \int_{380nm}^{780nm} I_\lambda \times z_\lambda$$

k is the constant for the measurement system, I_λ is the sample spectrum intensity, wavelength depending, x_λ, y_λ, z_λ are trichromatic values $x = X/(X + Y + Z)$, $y = Y/(X + Y + Z)$ and $z = Z/(X + Y + Z)$. Mean xyz values are given for each sample, which act as light sources (luminescent samples). Standards from Phosphor Technology used, calibrated at 312 nm: Gd_2O_2S:Eu, Gd_2O_2S:Tb.

Received: April 22, 2011
Published Online: July 22, 2011

